International Journal of Engineering and Management Sciences (IJEMS) Vol. 9. (2024). No. 2.
DOI: 10.21791/IJEMS.2024.017

Study on Nonlinear Behavior of Variable Thickness Plates

LAN HOANG THAT TON

University of Architecture, Faculty of Civil Engineering, HCM City. Vietnam. tltechonlinesom@gmail.com

Abstract. The analysis of variable-thickness plates is much more complicated than that of uniform-thickness plates because variable coefficients occur in the equations. In reality, this analysis is of great interest in various engineering disciplines, such as civil engineering, aerospace engineering, machine design, and so on. Although there is extensive literature on analyses of plates with constant thickness, a rather limited amount of technical literature is available on the solutions to problems dealing with plates with nonuniform thickness. The reason is that the analytical solutions meet insurmountable difficulties. Besides, the nonlinear analysis process also faces more difficulties than the linear analysis of structures. For these reasons, the nonlinear behavior of variable-thickness plates based on a finite element procedure is presented in this study. Although the topic is not special, it will help the engineer have a specific view of the nonlinear bending of the plate with variable thickness. This survey will be based on the change in geometrical parameters. Numerical solutions are then presented to verify the simplicity of this proposed procedure.

Keywords: Variable Thickness Plate, Nonlinear Bending, Finite Element Method

Introduction

Nowadays, variable-thickness plates are used in modern industries where different strengths and performances are exhibited in different parts of the product. Therefore, the study of nonlinear bending behavior is essential for practical needs. There have been some articles dealing with this issue. The literature [1] aimed at nonlinear bending analysis of tapered plates with variable thickness under 3D hygrothermal stresses related to Von Kármán theory. The different heat and moisture boundaries were also included in [1]. Based on eliminating singular sharp edges and a unified wavelet solving methodology, the governing partial differential equations for this structure in a hydro-thermo-mechanical environment have been given and solved. In [2], the bending problem of a thin plate with variable thickness under many kinds of boundary conditions was considered based on the meshless method related to weighted moving-least square approximation and the Taylor series. By introducing supplementary nodes on the boundary, this could treat the plates of complex shapes. A unified bran-new wavelet algorithm had been proposed for solving large bending of clamped or simply supported variable-thickness plates resting on nonlinear triparametric elastic foundations, as in [3]. The strongly nonlinear variable-coefficient governing equations for plates with variable thickness had been transformed and solved under the formulation of a thickness-distributed function meeting a circled homogeneous Neumann boundary. The dimensionless deflection was obtained by the wavelet homotopy approach. Nonlinear bending of prismatic, tapered, pitted, and raised plates was further investigated with different parameters of thickness profiles. In [4], by using displacement potential

DOI: 10.21791/IJEMS.2024.017

functions, the authors provided the results of bending of transversely isotropic thick rectangular plates with variable thickness. The governing partial differential equations were achieved by following the separation of variables method and this strategy had no limitation related to the boundary conditions or the change of thickness. The literature [5] gave a novel semi-analytical method for calculating variable thickness plates with various cutouts. Based on a finite sum of multiplications of one-dimensional functions as well as the variational extended Kantorovich method, the deflections were achieved. This way overcomed singularities at the cutout areas. The paper [6] introduced the bending behavior of variable-thickness thin rectangular plates under hygrothermomechanical influence. With the symbol "C" for clamped and "S" for simply supported, the CSCS plate in a hygrothermal environment was studied. The exact analytical solutions were given by using both the small parameter method and Lévy-type approach and so on. The nonlinear finite element procedure has also been mentioned by many documents, as in [7-9]. The authors in [7] gave the Matlab code for nonlinear analysis of isotropic plates, as well as in [8,9], based on the smoothed finite element method, the geometrically nonlinear behaviors of plates were also presented. This paper presents the simple strategy to get a specific view of the nonlinear behavior of variable thickness plates. This will be demonstrated in the following sections.

The next sections of this paper are given as follows. The brief of variable thickness plate and the finite element formulation for geometrically nonlinear analysis is presented in Sect.2. The numerical solutions are achieved and shown in Sect.3. Some concluding remarks are given in the last section.

1. Variable Thickness Plate And Finite Element Formulation

A variable-thickness plate is illustrated in Figure 1. The xy plane coincides with the mid-surface of this structure, while the z axis is perpendicular to the mid-surface.

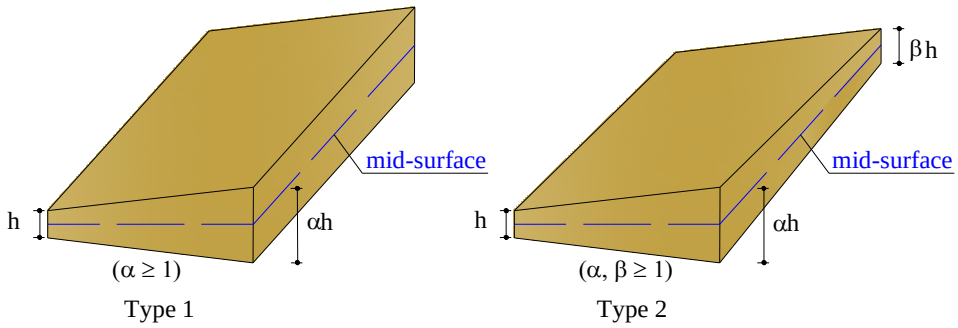

Figure 1. The variable thickness plates

Based on some literatures [7, 11, 12], the displacement field can be expressed as function of mid-surface translations u_o, v_o, w_o and mid-surface normal rotations θ_x, θ_y

$$\begin{aligned} \mathrm{u} &= -z\theta_x + u_o \\ \mathrm{v} &= -z\theta_y + v_o \\ \mathrm{w} &= w_o \end{aligned} \tag{1}$$

The strain vector is given by

DOI: 10.21791/IJEMS.2024.017

$$\varepsilon_x = \frac{\partial \mathrm{u}}{\partial x} + \frac{1}{2}\left(\frac{\partial \mathrm{w}}{\partial x}\right)^2, \quad \varepsilon_y = \frac{\partial \mathrm{v}}{\partial y} + \frac{1}{2}\left(\frac{\partial \mathrm{w}}{\partial y}\right)^2, \quad \gamma_{xy} = \frac{\partial \mathrm{u}}{\partial y} + \frac{\partial \mathrm{v}}{\partial x} + \frac{\partial \mathrm{w}}{\partial x}\frac{\partial \mathrm{w}}{\partial y}$$
$$\gamma_{xz} = \frac{\partial \mathrm{u}}{\partial z} + \frac{\partial \mathrm{w}}{\partial x}, \quad \gamma_{yz} = \frac{\partial \mathrm{v}}{\partial z} + \frac{\partial \mathrm{w}}{\partial y} \tag{2}$$

$$\boldsymbol{\varepsilon} = \begin{bmatrix} \varepsilon_x \\ \varepsilon_y \\ \gamma_{xy} \\ \gamma_{xz} \\ \gamma_{yz} \end{bmatrix} = \begin{bmatrix} \boldsymbol{\varepsilon}_m^L \\ 0 \end{bmatrix} + \begin{bmatrix} z\boldsymbol{\varepsilon}_b^L \\ \boldsymbol{\varepsilon}_s^L \end{bmatrix} + \begin{bmatrix} \boldsymbol{\varepsilon}_m^{NL} \\ 0 \end{bmatrix} \tag{3}$$

In which the linear membrane strains, the linear bending strains and shear strains are,

$$\boldsymbol{\varepsilon}_m^L = \begin{bmatrix} \frac{\partial \mathrm{u}}{\partial x} & \frac{\partial \mathrm{v}}{\partial y} & \frac{\partial \mathrm{u}}{\partial y} + \frac{\partial \mathrm{v}}{\partial x} \end{bmatrix}^T, \quad \boldsymbol{\varepsilon}_b^L = \begin{bmatrix} -\frac{\partial \theta_x}{\partial x} & -\frac{\partial \theta_y}{\partial y} & -\frac{\partial \theta_x}{\partial y} - \frac{\partial \theta_y}{\partial x} \end{bmatrix}^T, \quad \boldsymbol{\varepsilon}_s^L = \begin{bmatrix} \frac{\partial \mathrm{w}}{\partial x} - \theta_x & \frac{\partial \mathrm{w}}{\partial y} - \theta_y \end{bmatrix}^T \tag{4}$$

and the nonlinear membrane strains are,

$$\boldsymbol{\varepsilon}_m^{NL} = \begin{bmatrix} \frac{1}{2}\left(\frac{\partial \mathrm{w}}{\partial x}\right)^2 & \frac{1}{2}\left(\frac{\partial \mathrm{w}}{\partial y}\right)^2 & \frac{\partial \mathrm{w}}{\partial x}\frac{\partial \mathrm{w}}{\partial y} \end{bmatrix}^T \tag{5}$$

The stress resultant vector is then given,

$$\boldsymbol{\sigma} = \begin{bmatrix} \boldsymbol{\sigma}_m & \boldsymbol{\sigma}_b & \boldsymbol{\sigma}_s \end{bmatrix}^T \tag{6}$$

with,

$$\boldsymbol{\sigma}_m = \begin{bmatrix} N_x \\ N_y \\ N_{xy} \end{bmatrix} = \int_{-h/2}^{h/2} \begin{pmatrix} \sigma_x \\ \sigma_y \\ \sigma_{xy} \end{pmatrix} dz, \quad \boldsymbol{\sigma}_b = \begin{bmatrix} M_x \\ M_y \\ M_{xy} \end{bmatrix} = \int_{-h/2}^{h/2} \begin{pmatrix} \sigma_x \\ \sigma_y \\ \sigma_{xy} \end{pmatrix} z dz, \quad \boldsymbol{\sigma}_s = \begin{bmatrix} Q_{xz} \\ Q_{yz} \end{bmatrix} = \int_{-h/2}^{h/2} \begin{pmatrix} \tau_{xz} \\ \tau_{yz} \end{pmatrix} dz \tag{7}$$

Based on the combined membrane and bending part, the stress-strain relationship is,

$$\underbrace{\begin{bmatrix} N_x \\ N_y \\ N_{xy} \\ M_x \\ M_y \\ M_{xy} \end{bmatrix}}_{\boldsymbol{\sigma}_{mb}} = \underbrace{\frac{Eh}{\left(1-\nu^2\right)} \begin{bmatrix} 1 & \nu & 0 & 0 & 0 & 0 \\ \nu & 1 & 0 & 0 & 0 & 0 \\ 0 & 0 & \frac{\left(1-\nu\right)}{2} & 0 & 0 & 0 \\ 0 & 0 & 0 & \frac{h^2}{12} & \frac{h^2\nu}{12} & 0 \\ 0 & 0 & 0 & \frac{h^2\nu}{12} & \frac{h^2}{12} & 0 \\ 0 & 0 & 0 & 0 & 0 & \frac{h^2\left(1-\nu\right)}{24} \end{bmatrix}}_{\mathbf{D}_{mb}} \underbrace{\begin{bmatrix} \varepsilon_{xm} \\ \varepsilon_{ym} \\ \gamma_{xym} \\ \varepsilon_{xb} \\ \varepsilon_{yb} \\ \gamma_{xyb} \end{bmatrix}}_{\boldsymbol{\varepsilon}_{mb}} \tag{8}$$

The stress-strain relationship for shear part is,

$$\underbrace{\begin{bmatrix} Q_{xz} \\ Q_{yz} \end{bmatrix}}_{\boldsymbol{\sigma}_s} = \underbrace{k\frac{E}{2\left(1+\nu\right)}\begin{bmatrix} 1 & 0 \\ 0 & 1 \end{bmatrix}}_{\mathbf{D}_s} \underbrace{\begin{bmatrix} \gamma_{xz} \\ \gamma_{yz} \end{bmatrix}}_{\boldsymbol{\varepsilon}_s} \tag{9}$$

DOI: 10.21791/IJEMS.2024.017

where k = 5/6 is shear correction factor. The standard four-node quadrilateral isoparametric element is used for modeling as in Figure 2. For each element, the displacement vector $\boldsymbol{\varsigma}$ is given by,

$$\boldsymbol{\varsigma} = \{\varsigma_1 \quad \varsigma_2 \quad \varsigma_3 \quad \varsigma_4\}^T, \quad \varsigma_i = \begin{pmatrix} u_{oi} & v_{oi} & w_{oi} & \theta_{xi} & \theta_{yi} \end{pmatrix} \tag{10}$$

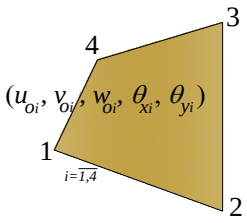

Figure 2. The standard four-node quadrilateral isoparametric element with five dofs per node

The first variation of potential energy leads to

$$\delta U = \delta W \tag{11}$$

in which the variation of strain energy of the plate is presented

$$\delta U = \int_A d\boldsymbol{\varepsilon}_{mb}^T \boldsymbol{\sigma}_{mb} dA + \int_A d\boldsymbol{\varepsilon}_s^T \boldsymbol{\sigma}_s dA \tag{12}$$

with

$$\begin{gathered} \boldsymbol{\varepsilon}_{mb} = \left(\mathbf{B}_{mb}^L + \frac{1}{2}\mathbf{B}_m^{NL} \right) \boldsymbol{\varsigma}, \quad \boldsymbol{\sigma}_{mb} = \mathbf{D}_{mb}\boldsymbol{\varepsilon}_{mb}, \quad d\boldsymbol{\varepsilon}_{mb} = \left(\mathbf{B}_{mb}^L + \mathbf{B}_m^{NL} \right) d\boldsymbol{\varsigma} = \mathbf{B}_{mb} d\boldsymbol{\varsigma} \\ \boldsymbol{\varepsilon}_s = \mathbf{B}_s^L \boldsymbol{\varsigma}, \quad \boldsymbol{\sigma}_s = \mathbf{D}_s \boldsymbol{\varepsilon}_s, \quad d\boldsymbol{\varepsilon}_s = \mathbf{B}_s^L d\boldsymbol{\varsigma} \end{gathered} \tag{13}$$

For non-linear analysis, [7, 9], the element equilibrium equation is

$$R = \int_A \mathbf{B}_{mb}^T \boldsymbol{\sigma}_{mb} dA + \int_A \mathbf{B}_s^T \boldsymbol{\sigma}_s dA - F = 0 \tag{14}$$

where R is residual and F is a generalized forces comes from variation of external work done. The element stiffness matrix $\mathbf{K}_S$ is written as

$$\begin{gathered} \mathbf{K}_S = \int_A \Psi dA + \int_A \Upsilon dA \\ \Psi = \left[\left(\mathbf{B}_{mb}^L \right)^T \mathbf{D}_{mb} \left(\mathbf{B}_{mb}^L \right) + \frac{1}{2} \left(\mathbf{B}_{mb}^L \right)^T \mathbf{D}_{mb} \left(\mathbf{B}_m^{NL} \right) + \left(\mathbf{B}_m^{NL} \right)^T \mathbf{D}_{mb} \left(\mathbf{B}_{mb}^L \right) + \frac{1}{2} \left(\mathbf{B}_m^{NL} \right)^T \mathbf{D}_{mb} \left(\mathbf{B}_m^{NL} \right) \right] \\ \Upsilon = \left(\mathbf{B}_s^L \right)^T \mathbf{D}_s \left(\mathbf{B}_s^L \right) \end{gathered} \tag{15}$$

The solution algorithm for the assembled nonlinear equilibrium equations as above is based on Newton-Raphson method which need linearization of equations at equilibrium point. The residual $R(\varsigma_{i+1})$ in the neighbourhood of ς_i by using the Taylor series expansion is

$$R(\varsigma_{i+1}) \approx R(\varsigma_i) + \mathbf{K}_T \Delta\varsigma = 0 \tag{16}$$

where $\mathbf{K}_T$ is assembled tangent stiffness matrix

$$\mathbf{K}_T = \mathbf{K}_{Lmb} + \mathbf{K}_{NLmb} + \mathbf{K}_\sigma + \mathbf{K}_{Ls} \tag{17}$$

in which the linear membrane-bending stiffness matrix

DOI: 10.21791/IJEMS.2024.017

$$\mathbf{K}_{Lmb} = \int_A \left(\mathbf{B}_{mb}^{L}\right)^T \mathbf{D}_{mb} \left(\mathbf{B}_{mb}^{L}\right) dA \tag{18}$$

the nonlinear membrane-bending stiffness matrix

$$\mathbf{K}_{NLmb} = \int_A \left[\left(\mathbf{B}_{mb}^{L}\right)^T \mathbf{D}_{mb} \left(\mathbf{B}_{m}^{NL}\right) + \left(\mathbf{B}_{m}^{NL}\right)^T \mathbf{D}_{mb} \left(\mathbf{B}_{mb}^{L}\right) + \left(\mathbf{B}_{m}^{NL}\right)^T \mathbf{D}_{mb} \left(\mathbf{B}_{m}^{NL}\right) \right] dA \tag{19}$$

the linear shear stiffness matrix

$$\mathbf{K}_{Ls} = \int_A \left(\mathbf{B}_{s}^{L}\right)^T \mathbf{D}_{s} \left(\mathbf{B}_{s}^{L}\right) dA \tag{20}$$

and the geometric matrix

$$\mathbf{K}_{Ls} = \int_A \left(d\mathbf{B}_{mb}\right)^T \boldsymbol{\sigma}_{mb} dA = \int_A \mathbf{G}^T \mathbf{N} \mathbf{G} dA \tag{21}$$

with

$$\mathbf{G} = \begin{bmatrix} 0 & 0 & \frac{\partial N_1}{\partial x} & 0 & 0 & \dots & 0 & 0 & \frac{\partial N_4}{\partial x} & 0 & 0 \\ 0 & 0 & \frac{\partial N_1}{\partial y} & 0 & 0 & \dots & 0 & 0 & \frac{\partial N_4}{\partial y} & 0 & 0 \end{bmatrix}_{2x20}, \quad \mathbf{N} = \begin{bmatrix} N_x & N_{xy} \\ N_{xy} & N_y \end{bmatrix} \tag{22}$$

Furthermore

$$\mathbf{B}_{mb}^{L} = \begin{bmatrix} \frac{\partial N_1}{\partial x} & 0 & 0 & 0 & 0 & \dots & \frac{\partial N_4}{\partial x} & 0 & 0 & 0 & 0 \\ 0 & \frac{\partial N_1}{\partial y} & 0 & 0 & 0 & \dots & 0 & \frac{\partial N_4}{\partial y} & 0 & 0 & 0 \\ \frac{\partial N_1}{\partial y} & \frac{\partial N_1}{\partial x} & 0 & 0 & 0 & \dots & \frac{\partial N_4}{\partial y} & \frac{\partial N_4}{\partial x} & 0 & 0 & 0 \\ 0 & 0 & 0 & -\frac{\partial N_1}{\partial x} & 0 & \dots & 0 & 0 & 0 & -\frac{\partial N_4}{\partial x} & 0 \\ 0 & 0 & 0 & 0 & -\frac{\partial N_1}{\partial y} & \dots & 0 & 0 & 0 & 0 & -\frac{\partial N_4}{\partial y} \\ 0 & 0 & 0 & -\frac{\partial N_1}{\partial y} & -\frac{\partial N_1}{\partial x} & \dots & 0 & 0 & 0 & -\frac{\partial N_4}{\partial y} & -\frac{\partial N_4}{\partial x} \end{bmatrix}_{6x20} \tag{23}$$

$$\mathbf{B}_{m}^{NL} = \begin{bmatrix} 0 & 0 & \frac{\partial w}{\partial x}\frac{\partial N_1}{\partial x} & 0 & 0 & \dots & 0 & 0 & \frac{\partial w}{\partial x}\frac{\partial N_4}{\partial x} & 0 & 0 \\ 0 & 0 & \frac{\partial w}{\partial y}\frac{\partial N_1}{\partial y} & 0 & 0 & \dots & 0 & 0 & \frac{\partial w}{\partial y}\frac{\partial N_4}{\partial y} & 0 & 0 \\ 0 & 0 & \frac{\partial w}{\partial y}\frac{\partial N_1}{\partial x} + \frac{\partial w}{\partial x}\frac{\partial N_1}{\partial y} & 0 & 0 & \dots & 0 & 0 & \frac{\partial w}{\partial y}\frac{\partial N_4}{\partial x} + \frac{\partial w}{\partial x}\frac{\partial N_4}{\partial y} & 0 & 0 \\ 0 & 0 & 0 & 0 & 0 & \dots & 0 & 0 & 0 & 0 & 0 \\ 0 & 0 & 0 & 0 & 0 & \dots & 0 & 0 & 0 & 0 & 0 \\ 0 & 0 & 0 & 0 & 0 & \dots & 0 & 0 & 0 & 0 & 0 \end{bmatrix}_{6x20} \tag{24}$$

DOI: 10.21791/IJEMS.2024.017

$$\mathbf{B}_s^L = \begin{bmatrix} 0 & 0 & \frac{\partial N_1}{\partial x} & -N_1 & 0 & \dots & 0 & 0 & \frac{\partial N_4}{\partial x} & -N_4 & 0 \\ 0 & 0 & \frac{\partial N_1}{\partial y} & 0 & -N_1 & \dots & 0 & 0 & \frac{\partial N_4}{\partial y} & 0 & -N_4 \end{bmatrix}_{2x20} \tag{25}$$

and $N_{i=1,2,3,4}$ are shape functions related to the standard four-node quadrilateral isoparametric element

2. Numerical Solutions

The numerical solutions for nonlinear analysis of variable thickness plates are presented. Firstly, to verify the correctness of this procedure to this structure, the simply supported (SSSS) square plate with a = 1, E = 10.92e9, ν = 0.3 and constant thickness $h = a/100$ is tested. The curve of maximum dimensionless deflections can be obtained by $\bar{\mathrm{w}} = \mathrm{w}_{\min} / h$ under load parameter $\bar{\mathrm{P}} = \left(Pa^4\right)/\left(Eh^4\right)$ and this curve is compared with the analytical solutions of Levy [10] in Figure 4. As can be seen from this figure, very good agreement is achieved for both ways. The first set of results corresponds to the mesh *6 x 6* and continues with the meshes *10 x 10, 14 x 14* and *18 x 18* as also shown in Figure 3 and Table 1, respectively.

$\bar{\mathrm{P}} = \left(Pa^4\right)/\left(Eh^4\right)$	$\bar{\mathrm{w}} = \mathrm{w}_{\min} / h$			
	6 x 6	*10 x 10*	*14 x 14*	*18 x 18*
0	0	0	0	0
9.157509	0.348498	0.347439	0.347118	0.346982
18.31502	0.567920	0.562144	0.560549	0.559893
27.47253	0.719531	0.709567	0.706872	0.705768
36.63004	0.836178	0.822742	0.819151	0.817686
45.78755	0.931820	0.915455	0.911117	0.909351
54.94505	1.013432	0.994543	0.989569	0.987546
64.10256	1.084980	1.063878	1.058349	1.056104
73.26007	1.148932	1.125862	1.119845	1.117404
82.41758	1.206933	1.182095	1.175639	1.173023
91.57509	1.260133	1.233691	1.226841	1.224068
100.7326	1.309373	1.281466	1.274257	1.271339
109.8901	1.355282	1.326030	1.318492	1.315442
119.0476	1.398349	1.367854	1.360012	1.356842
128.2051	1.438960	1.407311	1.399188	1.395905
137.3626	1.477422	1.444699	1.436314	1.432926
146.5201	1.513989	1.480262	1.471631	1.468145
155.6777	1.548869	1.514200	1.505340	1.501762
164.8352	1.582239	1.546684	1.537607	1.533943
173.9927	1.614246	1.577856	1.568574	1.564828
183.1502	1.645017	1.607837	1.598362	1.594538

Table 1. The value of $\bar{\mathrm{w}}$ *with four meshes*

DOI: 10.21791/IJEMS.2024.017

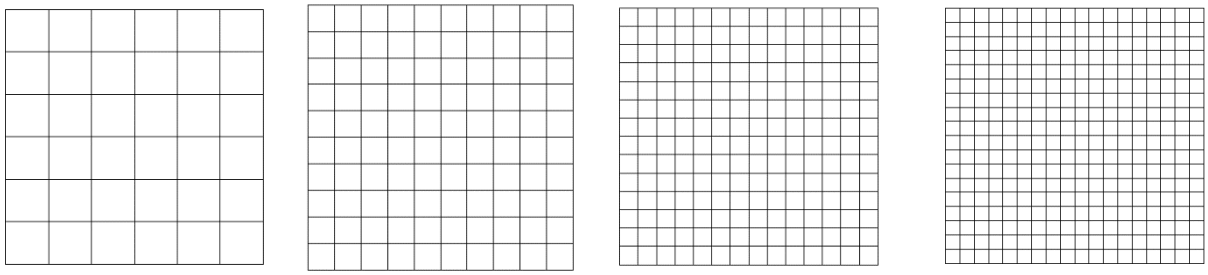

6 x 6 *10 x 10* *14 x 14* *18 x 18*

Figure 3. Four meshes of square plate

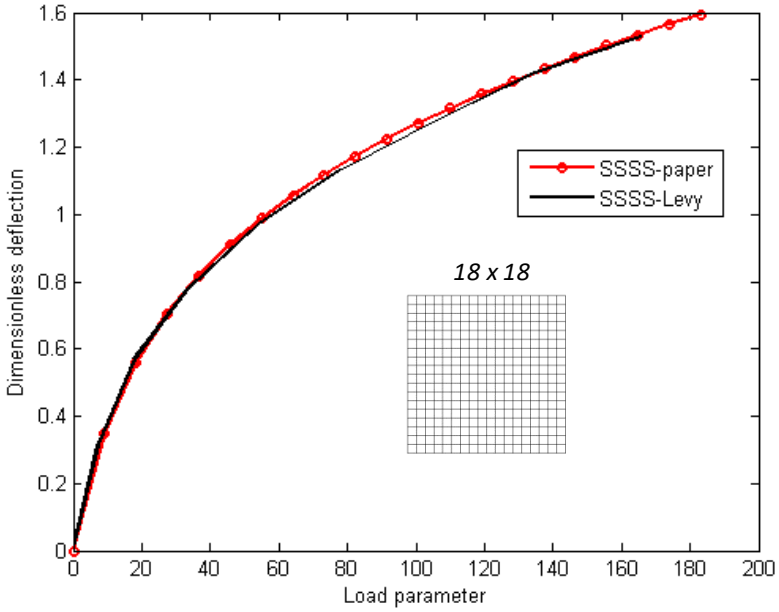

Figure 4. The comparison of dimensionless deflection with other literature

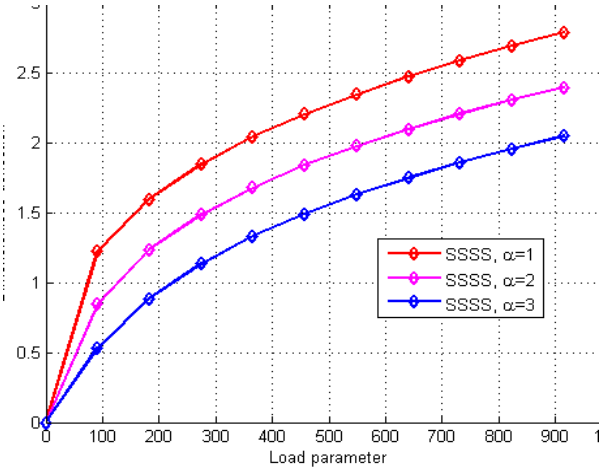

Type 1, SSSS

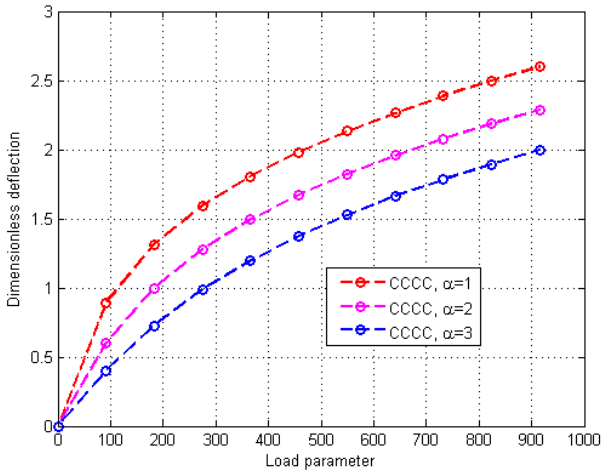

Type 1, CCCC

DOI: 10.21791/IJEMS.2024.017

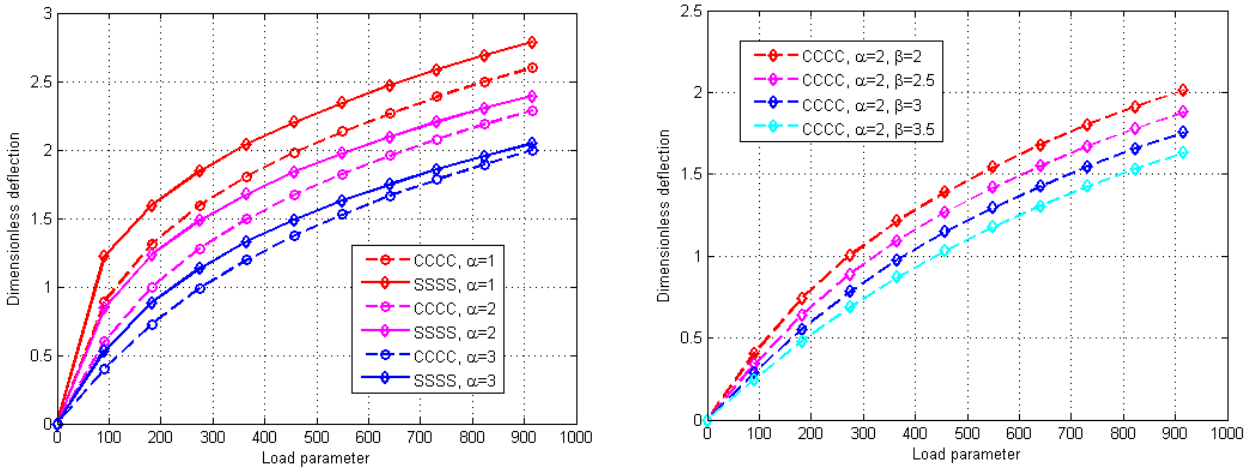

Type 1, CCCC & SSSS *Type 2, CCCC*

Figure 5. The curves of nonlinear bending with two types of plate by changing two geometrical parameters α and β

Finally, based on the above data as well as by changing two geometrical parameters α and β, the nonlinear behavior of variable thickness plates can be seen in Figure 5. For two kinds of boundary condition, fully simply supported (SSSS) and fully clamped (CCCC), an increase in these geometrical values increases the stiffness of the plate, resulting in a decrease in nonlinear deflection, respectively. From the above examples, it can be concluded that the present approach to the mechanical problem is reliable for analysing nonlinear behaviour of the variable thickness plate in terms of the bending problem and extending to others in future.

Conclusions

The analysis of variable-thickness plates is much more complicated than that of uniform-thickness plates because variable coefficients occur in the equations. In reality, this analysis is of great interest in various engineering disciplines. Although there is extensive work on the analysis of plates with constant thickness, a rather limited amount of technical investigation is available on the solution to variable-thickness plates. The reason is that the analytical solutions meet insurmountable difficulties. Besides, the nonlinear analysis process also faces more difficulties than the linear analysis of structures. For the above reasons, this paper is presented and deals with the nonlinear behavior of variable-thickness plates based on a simple approach related to the finite element method. The finite element consists of five degrees of freedom per node, which includes three displacements and two rotations. The computational approximation of this procedure is verified by comparing the obtained results with the results in other literature. The effect of the factor related to thickness on deflections is discussed. The success of the present flat four-node element provides a further demonstration of efficient flat elements for nonlinear analysis. The paper also helps to supplement the knowledge of engineers in design.

DOI: 10.21791/IJEMS.2024.017

References

[1] Q. Yu, "Large deflection bending analysis of variable-thickness tapered plates under three-dimensionally hygrothermomechanical loads," *International Journal of Mechanical Sciences*, vol. 207, p. 106648, 2021.

[2] F. Liu, L. Song, M. Jiang and G. Fu, "Generalized finite difference method for solving the bending problem of variable thickness thin plate," *Engineering Analysis with Boundary Elements*, vol. 139, pp. 69-76, 2022.

[3] Q. Yu, "Wavelet-based homotopy method for analysis of nonlinear bending of variable-thickness plate on elastic foundations," *Thin-Walled Structures*, vol. 157, p. 107105, 2020.

[4] F. Y. Tash and B. N. Neya, "An analytical solution for bending of transversely isotropic thick rectangular plates with variable thickness," *Applied Mathematical Modelling*, vol. 77, pp. 1582-1602, 2020.

[5] I. Shufrin and M. Eisenberger, "Semi-analytical modeling of cutouts in rectangular plates with variable thickness – Free vibration analysis," *Applied Mathematical Modelling*, vol. 40, pp. 6983-7000, 2016.

[6] A. M. Zenkour, "Bending of thin rectangular plates with variable-thickness in a hygrothermal environment," *Thin-Walled Structures*, vol. 123, pp. 333-340, 2018.

[7] A. Patil and S. S. Kolukula, "Fem Matlab code for linear and nonlinear bending analysis of plates," www.mathworks.com, 2016.

[8] X.Y. Cui, G. R. Liu, G. Y. Li, X. Zhao, T.T. Nguyen and G.Y. Sun, "A Smoothed Finite Element Method (SFEM) for Linear and Geometrically Nonlinear Analysis of Plates and Shells," *Computer Modeling in Engineering & Sciences*, vol. 28, pp. 109-126, 2008.

[9] L. T. That-Hoang, H. Nguyen-Van, T. Chau-Dinh and C. Huynh-Van, "Enhancement to four-node quadrilateral plate elements by using cell-based smoothed strains and higher-order shear deformation theory for nonlinear analysis of composite structures," *Journal of Sandwich Structures & Materials*, vol. 22, no. 7, pp. 2302-2329, 2020.

[10] S. Levy, "*Bending of Rectangular Plates with Large Deflections*," Report No. 737, NASA, 1942.

[11] H. Huo, Z. Liu, A. Xu, G. Chen and D. Yang, "Benchmark solutions for stochastic dynamic responses of rectangular Mindlin plates," *International Journal of Mechanical Sciences*, vol. 238, p. 107851, 2023.

[12] J. Chen, "The quadrilateral Mindlin plate elements using the spline interpolation bases," *Journal of Computational and Applied Mathematics*, vol. 329, pp. 68-83, 2018.